iScience

CellPress
OPEN ACCESS

Article

Analysis of microbiota reveals the underlying mechanism of PHF11 in the development of *Enterococcus*-regulated endometriotic cysts

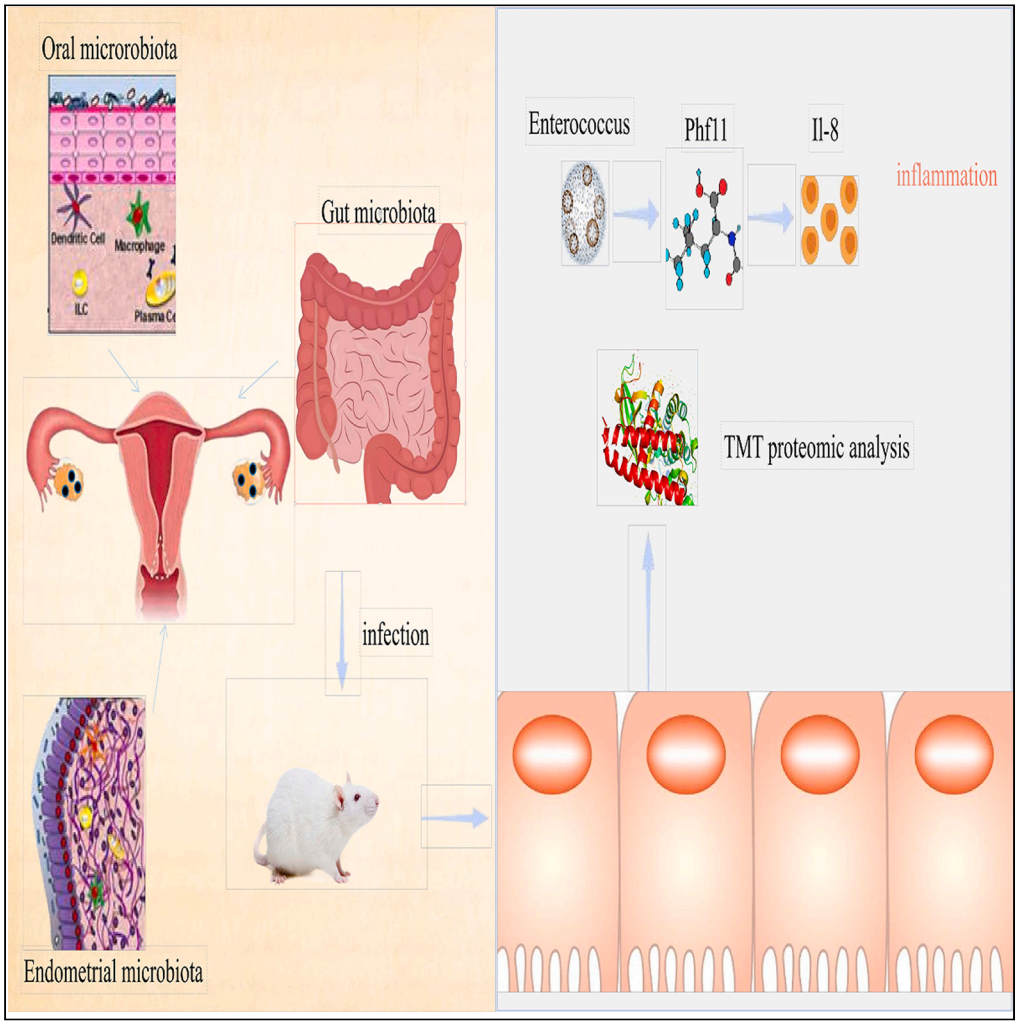

Jingjing Hu, Guanjian Li, Miaomiao Huang, ..., Yuqian Li, Yuan Fang, Yunxia Cao

caoyunxia5972@ahmu.edu.cn

Highlights

Microbiota composition of ectopic and eutopic tissues in EMS were different in richness

Gut microbiota of Enterococcus, Pseudomonas, Haemophilus and Neisseria were richness in EMS

Enterococcus-induced EMS mice presented higher lesion infiltration

PHF11 was downregulated in the Enterococcus-induced mice, but upregulated of IL-8

Hu et al., iScience *26*, 108158
November 17, 2023
https://doi.org/10.1016/j.isci.2023.108158

iScience

CellPress
OPEN ACCESS

Article

Analysis of microbiota reveals the underlying mechanism of PHF11 in the development of *Enterococcus*-regulated endometriotic cysts

Jingjing Hu,[1,2,3,8] Guanjian Li,[1,2,3,8] Miaomiao Huang,[1,2,3,8] Qunshan Shen,[1,2,3,8] Hao Gu,[4,8] Nairui Xue,[1,2,3,8] Junqiang Zhang,[1,2,5] Xiaofeng Xu,[1,2,5] Wenjuan Yang,[1,2,6] Aying Xing,[1,2,6] Xiao Wu,[1,2,6] Ying Wang,[1,2,6] Rong Wu,[1,2,6] Chuan Xu,[1,2,6] Yuqian Li,[1,2,7] Yuan Fang,[1,2,7] and Yunxia Cao[1,2,3,9,*]

SUMMARY

Endometriosis (EMS) is a prevalent disease and the etiologies has not uniform. Microbiota is associated with human diseases. To delve into the relationship between EMS and microbiota, Ectopic (EM) and eutopic (EU) endometrial tissues, pharyngeal swabs, and stools were collected from EMS patients. The microbiota composition of EM and EU partially overlapped, with similar taxon numbers and diversity, but the richness levels were significantly different. A comparison of intestinal microbes in healthy individuals (FN) and EMS patients (FE) revealed that the richness of Enterococcus, Pseudomonas, Haemophilus, and Neisseria was enhanced in FE. In addition, Enterococcus-induced mice (EFA) presented with a higher degree of lesion infiltration and a wider distribution of lesions. Proteomic analysis revealed the expression of plant homeodomain finger 11 (PHF11) was notably downregulated in EFA. And the downregulated expression of PHF11 was accompanied by the upregulated expression of interleukin 8 (IL-8). Our findings suggest a potential regulatory mechanism for PHF11 in EMS development.

INTRODUCTION

Endometriosis (EMS) develops when endometrial tissues with growth functions are present outside the mucosal lining of the uterine cavity. Pathologically, the disease may manifest as ovarian (an endometriotic cyst), peritoneal, or infiltrative EMS or adenomyosis, among which an endometriotic cyst, a type of ovarian tumor, is the most common. EMS is prevalent among women of childbearing age. In recent years, the incidence has exhibited a younger trend, and morbidity continues to increase annually, reaching 10–15%. In addition, 30–40% of gynecological disease-related surgeries are performed to treat EMS.[1] As a benign gynecological disease, it also demonstrates malignant behaviors such as invasion and implantation, with a cancer rate of 0.7–1.0%.

Several high-risk factors are associated with the disease: (1) immune dysfunction: EMS is possibly an autoimmune disease, as the patients usually suffer from local/systemic abnormalities in cellular or humoral immune function; (2) menstrual abnormalities: the onset of EMS is often accompanied by an excessive volume of menstrual blood; (3) genetic factors: patients with a positive family history of EMS are younger when the disease occurs and experience more severe symptoms, suggestive of familial aggregation and an association between the disease and genetic factors. The genes responsible for the development of EMS and ovarian tumors are homologous.[2] Currently, not all hypotheses on EMS etiologies yield a convincing conclusion, and the pathogenesis remains ambiguous. Menstrual blood reflux is considered a potential trigger, and immune system dysfunction is a significant factor.[3] Ectopically implanted endometrium is as invasive as malignant cells, and the invasion process primarily comprises of three steps: adhesion, angiogenesis, and implantation.[4] Immune mechanisms are involved in invasion via numerous adhesion molecules, enzymes, and angiogenic factors, which usually lead to an abnormal immune system, inducing abnormalities in immune functions. Immunoreactive cells in the abdominal cavity, including macrophages, natural killer (NK) cells, T cells, and B cells, constitute the first line of defense in the human abdominal cavity. These cells are released into ascites together with endometriotic cells, cytokines, and inflammatory mediators (such as interleukin-8 [IL-8], transforming growth factor β [TGF-β], Tumor necrosis factor alpha [TNF-α],

[1]Department of Obstetrics and Gynecology, The First Affiliated Hospital of Anhui Medical University, No 218 Jixi Road, Hefei, Anhui 230022, China
[2]NHC Key Laboratory of Study on Abnormal Gametes and Reproductive Tract (Anhui Medical University), No 81 Meishan Road, Hefei, Anhui 230032, China
[3]Key Laboratory of Population Health Across Life Cycle (Anhui Medical University), Ministry of Education of the People's Republic of China, No 81 Meishan Road, Hefei, Anhui 230032, China
[4]School of Basic Medical Sciences, Anhui Medical University, Hefei, Anhui 230022, China
[5]Engineering Research Center of Biopreservation and Artifical Organs, Ministry of Education, No 81 Meishan Road, Hefei, Anhui 230032, China
[6]Anhui Province Key Laboratory of Reproductive Health and Genetics, No 81 Meishan Road, Hefei, Anhui 230032, China
[7]Biopreservation and Artificial Organs, Anhui Provincial Engineering Research Center, Anhui Medical University, No 81 Meishan Road, Hefei, Anhui 230032, China
[8]These authors contribute equally
[9]Lead contact
*Correspondence: caoyunxia5972@ahmu.edu.cn
https://doi.org/10.1016/j.isci.2023.108158

Table 1. Intergroup comparison of basic data

Variables	EMS (n = 14)	CON (n = 24)	P-value
Age, years	30.64 (29.25–32.03)	29.38 (28.39–30.36)	0.119
BMI, kg/m^2	20.29 (19.12–21.46)	22.75 (21.23–24.27)	0.010
CA125, U/mL	49.98 (34.85–65.11)	15.72 (12.94–18.49)	0.000

and epidermal growth factor receptor [EGFR]),[5,6] resulting in permeability changes in the local peritoneal environment and eventually triggering endometrial implantation.

As a neutrophil-activating factor, IL-8 was one of the first pro-inflammatory chemokines identified. Mainly generated by neutrophils, monocytes, macrophages, T lymphocytes, epithelial cells, and endothelial cells, IL-8 regulates cell proliferation and differentiation, facilitates the production of inflammatory proteins, and induces angiogenesis, playing a vital role in the progression of EMS.[7] Thus, IL-8 is favorable for the survival and proliferation of ectopic endometrium. In fact, elevated IL-8 levels and disease severity are associated with lesion size and activity. Additionally, IL-8 is expressed in the endometrial stroma as an autocrine growth factor that promotes the proliferation of stromal cells from endometriotic tissues and indirectly protects them from apoptosis.[8] Collectively, IL-8 protects ectopic cells from apoptosis and induces the development and progression of EMS by facilitating endometrial cell attachment, thereby playing a role in EMS pathogenesis.

The human body is colonized by diverse symbiotic and pathogenic microbiota including bacteria, archaea, fungi, protists, and viruses. The entire habitat that encompasses such microbes, their genomes, and their surroundings is known as the microbiome.[9] Different microbiota involved in various functions from metabolism to immunity are crucial to human health. The human microbiota and metagenome play key roles in maintaining body homeostasis and in the development of certain diseases (including cancer). In a microbiota, through mutual adaptation and natural selection between different microbes, as well as between microbes and the host, the three elements are in a balanced state and play an irreplaceable role in human digestive, metabolic, and immune functions.[10,11] Currently, compelling evidence has demonstrated that the human microbiome is vital for the development of multiple tumors and oral, reproductive, and neurological diseases. In addition, over 16% of cancer incidence is attributed to infectious agents, and intratumoral bacteria have been reported in multiple tumor types. However, these bacterial types have not yet been standardized.

The gut microbiota affects various aspects of tumor biology such as the transformation process, tumor progression, and anticancer immunotherapy.[12] In this context, characterization of the tumor microbiome may be crucial for revealing the impact of bacteria on different cancers. The oral cavity is the starting site of the human gastrointestinal and respiratory tracts, where more than 700 types of bacteria can be found.[13] According to colonization site, microbiota can be classified as gut, respiratory, genitourinary, or skin microbial flora. Adequate microbiome research based on microbiota classification can further facilitate the understanding of the pathogenesis of various diseases, thus bringing about new diagnostic approaches. Recently, the effects of the reproductive tract and gut microbiome on female reproductive diseases have been explored.[13] However, few researchers have investigated female reproductive diseases from the perspective of the tumor tissue microbiome. As ovarian endometriotic cysts are a prevalent type of gynecological tumor that possess malignant features, the microbial environment of tumor tissues in patients with ovarian endometriotic cysts should be investigated to elucidate the link between the two and any underlying molecular mechanisms.

Therefore, the present study aimed to investigate the composition characteristics of the microbiota in different body parts of EMS patients, analyze the differences in gut microbiota richness between EMS patients and healthy controls, establish and analyze EMS murine models with different microbes, and explore their biological mechanisms.

RESULTS

Participant characteristics

Fourteen patients with endometriotic cysts (EMS group) and 24 healthy controls were included in this study. All patients with EMS were at disease stages III-IV, as confirmed by r-ASRM. The clinical characteristics of the enrolled patients are shown in Table 1. For participants from EMS and control groups, their median ages were 30.64 (29.25–32.03) and 29.38 (28.39–30.36) years, respectively; the median body mass indices (BMIs) were 20.29 (19.12–21.46) and 22.75 (21.23–24.27) kg/m^2, respectively; and the median cancer antigen 125 (CA125) levels were 49.98 (34.85–65.11) and 15.72 (12.94–18.49), respectively (Table 1). The CA125 levels in the EMS group were significantly higher than those in the control group ($p < 0.05$).

Four samples from different body parts were obtained from each patient with EMS, whereas only one sample was collected from each healthy control; ultimately, 72 qualified samples were successfully acquired from the patients with EMS and control participants, categorized into 5 groups (FE, FN, EM EU, and OM). 16S rRNA gene sequencing was conducted on all samples to determine the microbial features of different tissue samples in all participants. By analyzing α-diversity dilution and hierarchical clustering curves, the species in the sequenced samples were revealed to be uniformly distributed with high richness (Figures 1A and 2A). The number of sequences can be used for relevant data analysis.

The bacterial composition of each sample was evaluated using the diversity indices based on different OTUs (α-diversity). The EM and EU groups exhibited no differences in the Shannon and Simpson indices, and no abnormalities were observed in either group in terms of microbiota diversity or uniformity (Figure 1B). The Shannon and Simpson indices of the FE and FN groups were significantly different ($p < 0.05$), and

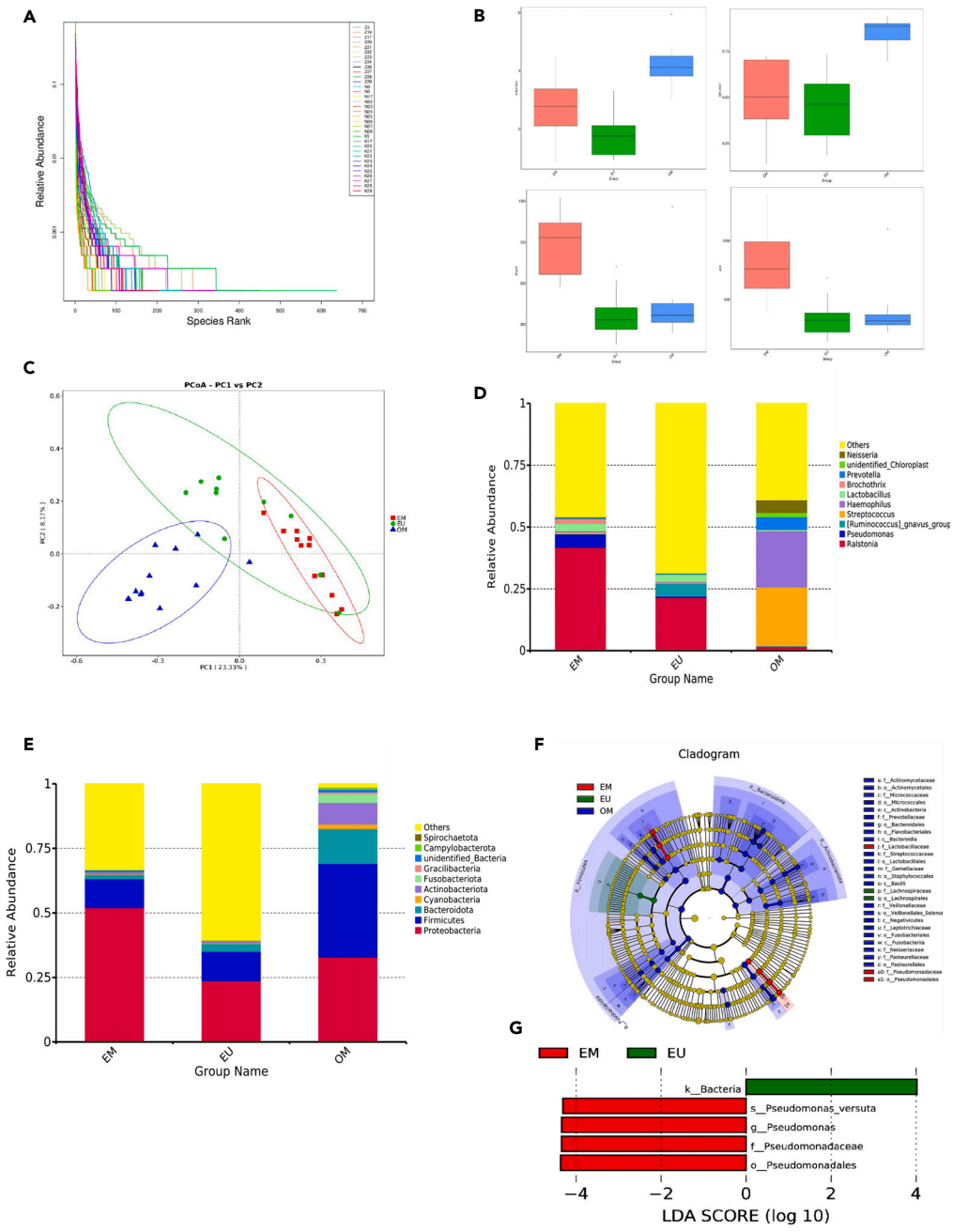

Figure 1. Distribution characteristics of EMS microflora in different body parts

(A) Rank Abundance curve. The abscess is the serial number ranked by OTUs abundance, and the ordinate is the relative abundance of OTUs. Different samples are represented by broken lines in different colors.

(B) In the analysis of intergroup differences of Alpha diversity index, the box graph can directly reflect the median, dispersion, maximum, minimum, and outlier values of species diversity within the group. A Wilcox rank-sum test was used to analyze Shannon, Simpson, Chao1, and ACE index differences among the groups; $p < 0.05$ was considered statistically significant.

(C) Two-dimensional PCoA analysis. The abscissa represents one principal component, the ordinate represents the other principal component, and the percentage represents the contribution value of the principal component to the sample composition difference. The closer the two sample points are, the more similar the species composition of the two samples.

(D) Histogram of relative abundance of EM, EU, and OM species at the phylum level.

(E) Histogram of relative abundance of EM, EU, and OM species at the genus level.

(F) In this cladistic diagram, inside-out represents the taxonomic level from phylum to genus (or species). Each small circle at a different classification level represents a classification at that level, and the diameter is proportional to the relative abundance. The color of species with no significant difference was

Figure 1. *Continued*
yellow, and the color of different species Biomarker following group was red, green, and blue, respectively. Nodes represent important microbial groups in this group.
(G) EM at the genus level; histogram of the distribution of linear discriminant analysis (LDA) values in the EU group, showing the significant role of the microbiome in both groups (species with an LDA score greater than the set value (default setting = 4)); the length of the histogram represents the magnitude of the influence of different species.

the microbes in the FN group were more diverse with a more concentrated distribution (Figure 2B). In addition, the microbiota of the OM group showed higher richness and diversity, presenting significant differences compared with the other groups (Figure 1B).

Comparison of microflora from different body parts of patients with EMS

At the phylum level, the top 10 microbes with the highest richness in the EM, EU, and OM groups were Proteobacteria, Firmicutes, Bacteroides, Actinobacteria, Cyanobacteria, Fusobacteria, Phylum Gracilicutes, Campylobacterota, and spiral bacteria. Proteobacteria, Firmicutes, and Bacteroides were among the top three microbes in terms of richness in the three groups (Figure 1D). In the EM group, the richness of the three microbes was 51.90%, 11.21%, and 1.61%, respectively. In the EU group, the richness was 23.70%, 11.41%, and 3.02%, respectively. In the OM group, the richness increased to 32.84%, 36.35%, and 13.48%, respectively. At the genus level, the top 10 microbes with the highest richness in the EM, EU, and OM groups were *Ralstonia*, *Neisseria*, *Pseudomonas*, *Ruminococcus gnavus*, *Streptococcus*, *Lactobacillus*, *Prevotella*, *Escherichia*, and *Haemophilus parasuis*. In the EM group, the three microbes with the highest genus-level richness were *Ralstonia* (41.75%), *Pseudomonas* (5.47%), and *Lactobacillus* (3.07%), among which *Ralstonia* and *Pseudomonas* are Proteobacteria and *Lactobacillus* is a Firmicutes. In the EU group, the three microbes with the highest genus richness were *Ralstonia* (21.53%), *Ruminococcus gnavus* (5.17%), and *Lactobacillus* (2.93%). In the OM group, the three microbes with the highest genus richness were *Streptococcus* (23.56%), *Haemophilus parasuis* (22.67%), and *Prevotella* (5.18%) (Figure 1E). Through pairwise comparisons in PCoA based on the Bray-Curtis distance, the microbiota composition of the EM group was discovered to be more concentrated and partially coincided with that of the EU group but did not overlap with that of the OM group (Figure 1C). In addition, the microbiota composition of the OM group was more diverse, exhibiting visible differences compared to that of the other two groups (Figure 1F). The t-test for each taxon at the phylum level indicated that Pseudomonas richness was higher in the EM group than in the EU group (Figure 1G).

Gut microbiota differences between EMS and control groups

The top three microbes in both the FE and FN groups were Firmicutes (45.70% and 65.57%, respectively), *Bacteroides* (20.72% and 9.39%, respectively), and Proteobacteria (16.87% and 6.58%, respectively) (Figures 2D and 2E). In the two groups, Firmicutes richness was significantly lower and Proteobacteria richness was markedly higher in FE group. Ranked by genus richness, the top 10 microbes in the FE and FN groups were *Enterococcus*, *Prevotella*, *Bacteroides*, *Ralstonia*, *Actinomyces*, *Ruminococcus gnavus*, *Lactobacillus*, *Enterobacter*, *Escherichia*, and *Bifidobacterium*. In the FE group, the richness of *Bacteroides*, *Escherichia coli*, and *Bifidobacterium* (5.71%, 0.94%, and 0.59%, respectively) was lower than that in the FN group (15.48%, 4.72%, and 4.19%, respectively), whereas the richness of *Enterococcus* (8.62%) was higher than that in the FN group (0.23%). The richness of *Ralstonia* and *Prevotella* in the FN group was zero (Figure 2F). By analyzing the microbial differences with PCoA based on the Bray-Curtis distance, the microbiota composition of the FE group was found to be more concentrated and partially coincided with that of the FN group, with several samples exhibiting unique microbiota composition (Figure 2C). At the genus level, the abundance of *Enterococcus*, *Prevotella*, *Ralstonia*, *Asteroleplasma*, *Lactobacillus*, *Haemophilus*, and *Ruminococcus gnavus* increased in the FE group, whereas in the FN group, the abundance of *Blautia*, *Bacteroides*, *Faecalibacterium*, *Bifidobacterium*, *Escherichia-Shigella*, *Eubacterium*, *Fusicatenibacter*, and *Collinsella* increased (Figure 2G). A t-test of different microorganisms at the genus level showed that the richness of *Bacteroides* ($p = 0.004$), *Escherichia coli* ($p = 0.044$), and *Bifidobacterium* ($p = 0.006$) in the FN group significantly increased, whereas that of *Enterococcus* ($p = 0.016$), *Prevotella* ($p < 0.000$), and Rawlsia ($p < 0.000$) in the FE group increased. This difference was statistically significant ($p < 0.05$) (Figure 2G).

Functional annotation of the ten microbes with highest richness from participants of the EMS and control groups

By comparing the whole-genome sequences of prokaryotes obtained through 16S rRNA analysis based on the 16S Silva database, the metabolic and functional differences caused by microbes between different groups were screened. The top 35 functions were selected and combined with the species richness in the samples to illustrate a functional heatmap. Clustering performed at the level of functional differences showed that in the EM group, decarboxylative metabolism of glyoxylate, oxidative stress phosphorylation, bacterial kinetic protein function, and glycine-serine-threonine metabolism were enhanced, whereas peptidoglycan synthesis and protein degradation were weakened. In the EU group, mitochondrial biological functions were greatly strengthened. In the FE group, the carbon fixation pathway, alanine-aspartate-glutamate, and peptidase functions were significantly enhanced, whereas pyruvate and mitochondrial functions were markedly reduced (Figure 2H).

Animal model analysis

The 15 recipient mice were stratified into control (CON), EFA, and EFV groups. During the modeling process, all mice in the three groups survived with no obvious infection at the injection sites. On the 7th post-modeling day, the mice were euthanized by cervical dislocation (Figure 3A), followed by laparotomy to detect the formation, morphology, site, and adhesion conditions of the ectopic lesions. These lesions were observed in mice in all three groups (Figure 3B). Each lesion was transparent and cystic in a spherical shape with increasing volume and

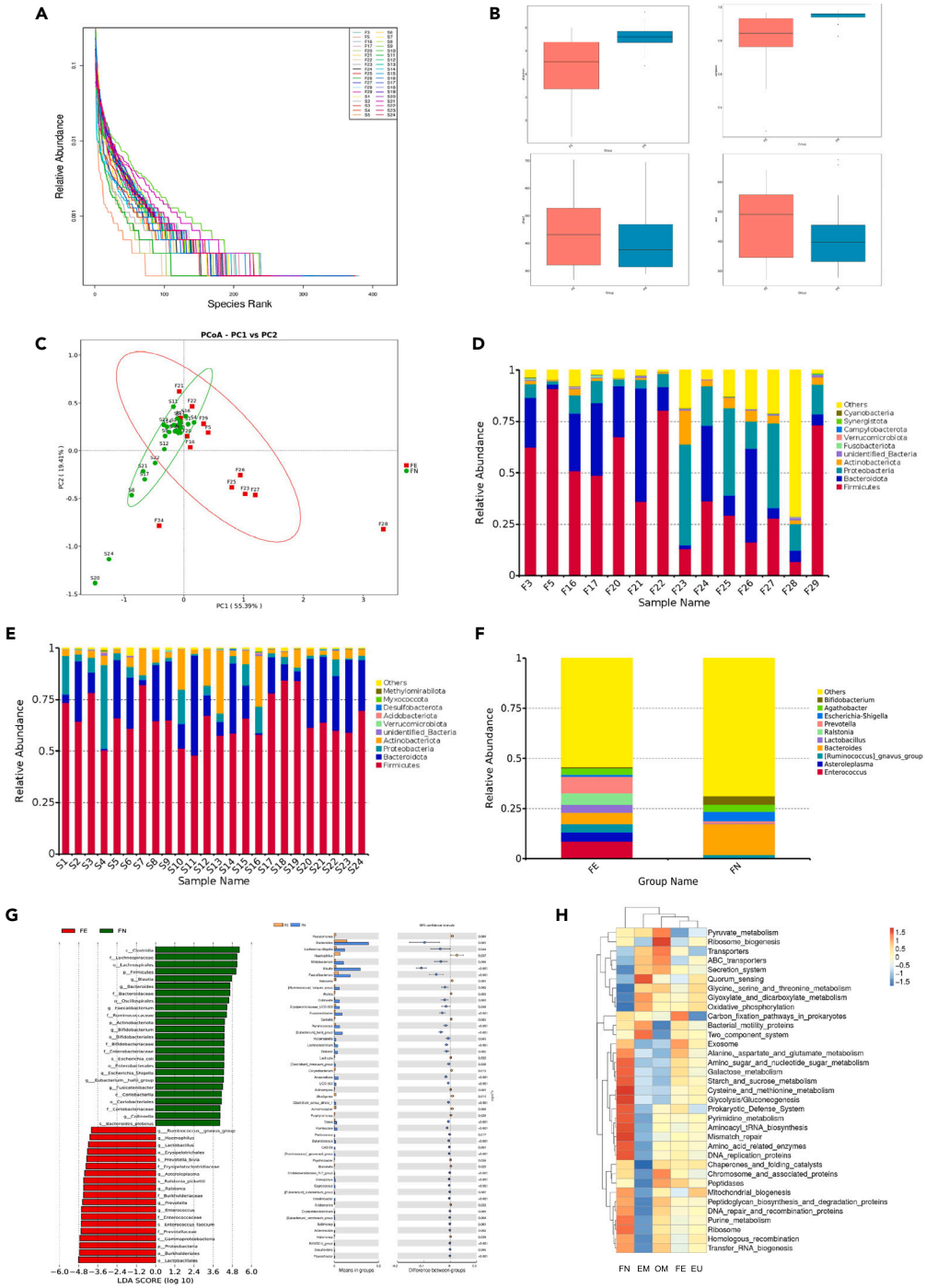

Figure 2. Distribution characteristics of intestinal microflora in the EMS and control groups

(A) Rank Abundance curve. The abscess is the number ranked by OTU abundance, and the ordinate is the relative abundance of the OTUs. Different samples are represented by broken lines in different colors.

(B) In α-diversity analysis indexes of intergroup difference, the box graph represents the median, dispersion, maximum, minimum, and outlier values of species diversity within the group. A Wilcox rank-sum test was used to analyze the Shannon, Simpson, Chao1, and ACE index differences among the groups; $p < 0.05$ was considered statistically significant.

(C) Two-dimensional PCoA analysis. The abscissa represents one principal component, the ordinate represents the other principal component, and the percentage represents the contribution value of the principal component to the sample composition difference. The closer the two sample points are, the more similar the species composition of the two samples.

(D) Histogram of the top 10 species in the FE group at the phylum level.

Figure 2. *Continued*

(E) Histogram of the top 10 species in relative abundance of the FN group at genus level.

(F) FE and FN column graphs of the top 10 species in the relative abundance of microorganisms at the genus level.

(G) Histogram of LDA value distribution of EM at the level of the EU group shows the microflora with significant effects in the two groups (species with an LDA score greater than the set value (default setting = 4)). The length of the histogram represents the influence of different species. For the different species between groups, a t-test between groups was performed (p value <0.05); the confidence interval and p value are shown on the right.

(H) The top 35 functions with the highest abundance and their abundance information in each group were selected to draw heat maps. The clustering was carried out from the level of functional differences.

gray-white cystic-solid projections. Inside the lesion was a yellow liquid with small nascent vessels on its surface. Each control mouse had a single lesion with a diameter of approximately 4 mm, mostly located on the surface of the intestinal canal. The EFA mice exhibited a significantly enlarged lesion scope, with many lesions observed in the intestinal canal, peritoneum, and omentum. Heterogeneous blood vessels were extremely abundant, and adhesion of the three parts was visible. The largest lesion measured approximately 11 mm in diameter (Figure 3C). Among the EFV mice, most lesions were located in the intestinal canal, whereas some were in the peritoneum, with the maximum lesion diameter reaching approximately 7 mm. Peritoneal adhesions were also observed. The endometrial tissue blocks from each group were dissected and weighed (Figure 3D). The tissue weights of samples from the CON, EFA, and EFV groups were 30.38 ± 20.50 (mg, s), 133.62 ± 83.21 (mg, s), and 81.60 ± 73.60 (mg, s) (Table 2), respectively. Analysis of variance (ANOVA) of tissue weights indicated differences among the three groups in terms of tissue weight ($p = 0.037$, $p < 0.05$). The tissue weight differences were statistically significant between the CON and EFA groups ($p = 0.016$, $p < 0.05$), and between the EFA and EFV groups ($p = 0.049$, $p < 0.05$). However, no statistically significant difference in tissue weight was observed between the CON and EFV groups ($p = 0.544$, $p > 0.05$) (Figure 3E).

Quality control of protein samples

After protein extraction from murine tissue samples, protein concentrations were measured, and SDS-PAGE was conducted, which showed that the sample bands were clear and parallel, meeting the mass spectrometry criteria. Through TMT protein quantification technique and tandem mass spectrometry analysis, a total of 60,959 peptides and 7,177 proteins were identified, which were subsequently analyzed with the criteria of FC $\geq$ 1.5 or $\leq$1/1.5 and p value <0.05 (Figure 4A).

Identification and bioinformatic analysis of DEPs

Compared to the proteins identified in the CON group, 103 proteins were upregulated and 165 were downregulated in the EFA group. In the EFV group, 314 were upregulated and 231 were downregulated. Compared to the EFV group, the EFA group possessed only 3 proteins with upregulated expression and 84 with downregulated expression (Figures 4B–4D).

GO classification enrichment analysis of DEPs demonstrated that these proteins were primarily involved in biological processes (BPs), cellular components (CCs), and molecular functions (MFs). The EFA-CON proteins with upregulated expression, mainly concentrated in the cytoplasmic membrane, extracellular membrane, and cell surface of CCs, were involved in fatty acid metabolism and positive regulation of inflammatory responses(Figure 4E), whereas the proteins with downregulated expression were located in the mitochondria, chromatin, and nuclear matrix of CCs, with MFs showing protein homodimerization activity, actin filament binding, and nuclear receptor co-activation activity(Figure 4F). In contrast, EFV-CON proteins with upregulated expression, mainly concentrated in the extracellular voids, cell surface, external side of the plasma membrane, and collagen-containing extracellular matrix (ECM) of CCs, regulated innate immune responses and viral and bacterial defense responses and participated in signal receptor binding, heparin binding, and double-stranded RNA binding with serine-type endopeptidase inhibitor activity(Figure 4G), whereas proteins with downregulated expression, which were primarily located in the mitochondria and inner mitochondrial membrane of CCs, modulated the assembly of mitochondrial respiratory complex I, mitochondrial electron transport, and tricarboxylic acid cycle(Figure 4H). The EFA-EFV proteins with downregulated expression were mainly responsible for the modulation of innate immune functions and defense against viruses and bacteria (Figure 4I).

KEGG pathway analysis demonstrated that the upregulated EFA-CON proteins were enriched in oxidative activation signaling pathways, lipolysis, bacterial infection, and hematopoietic/immune system diseases, whereas the downregulated proteins were enriched in diabetes, cardiomyopathy, oxidative phosphorylation, hematopoietic/immune system diseases, and B cell receptor signaling pathways (Figure 4J). The upregulated expression of EFV-CON proteins was enriched in the complement system, cholesterol metabolism, COVID-19, and oxidative activation signaling pathways, whereas the proteins with downregulated expression were enriched in oxidative phosphorylation, diabetes, cardiomyopathy, reactive oxygen carcinogenesis, and parkinsonism (Figure 4K). Moreover, EFA-EFV proteins with downregulated expression were enriched in viral infections such as measles, influenza, COVID-19, necrosis, and apoptosis (Figure 4L).

Screening of DEPs

The above analyses indicated a trend of downregulated expression for most core EFA-EFV proteins. The top 10 proteins with the most significantly downregulated expression were interferon induced protein with tetratricopeptide repeats 2 (Ifit2), Ifit3, Ifit1, membrane-spanning 4-domains subfamily A member 6C (Ms4a6c), lymphocyte antigen 6 complex, locus A (Ly6a), plant homeodomain finger protein 11 (PHF11), ISG15 ubiquitin like modifier (Isg15), radical S-adenosyl methionine domain containing 2 (Rsad2), and lymphocyte antigen 6 complex, locus C1 (Ly6c1). Compared to the CON, PHF11 was downregulated in the EFA group (FC, 0.54) but was upregulated in the EFV group (FC,

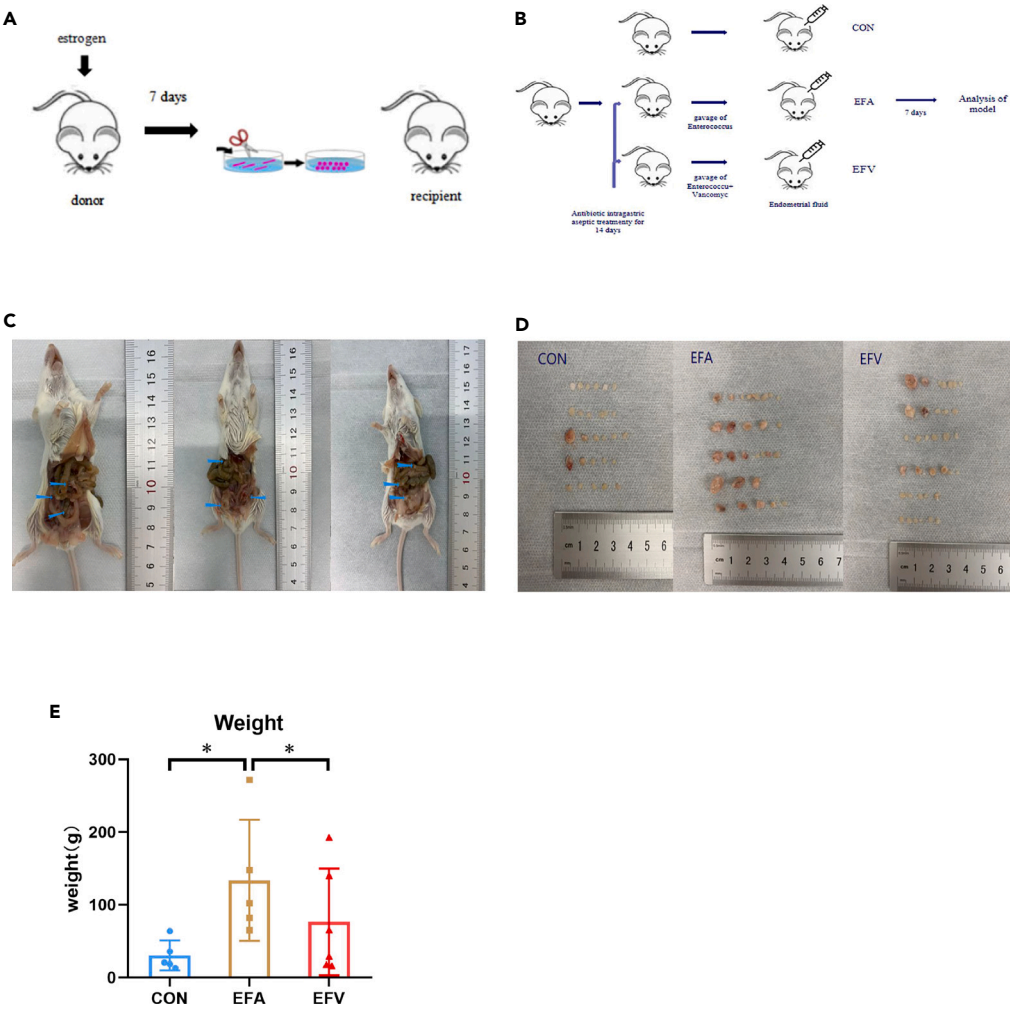

Figure 3. Analysis of lesions in an Enterococcus-induced mouse model of EMS

(A) Donor mouse model.

(B) Recipient mouse model.

(C) The anatomical image of the EMS mouse model showed that the ectopic lesion was located on the surface of the intestinal tube in a follicular shape and formed local adhesion and nodules in the greater omentum and mesentery.

(D) Schematic diagram of ectopic lesion tissue blocks in CON, EFA, and EFV mice.

(E) Ectopic tissue weight of samples from CON, EFA, and EFV mice; $p < 0.05$ was considered statistically significant.

1.83). The PPI network analysis revealed the 38 proteins most strongly associated with PHF11, including adenosine deaminase RNA specific (Adar), bone marrow stromal cell antigen 2 (Bst2), cytidine/uridine monophosphate kinase 2 (Cmpk2), death domain associated protein (Daxx), RNA sensor RIG-I (Ddx58), deltex E3 ubiquitin ligase 3 L (Dtx3l), eukaryotic translation initiation factor 2 alpha kinase 2 (Eif2ak2), interferon activated gene 205 (Ifi205a), interferon induced protein 44 (Ifi44), interferon induced protein 44 like (Ifi44l), interferon induced with helicase C domain 1 (Ifih1), Ifit1, Iifit2, Iifit3, Isg15, Isg20, galectin 3 binding protein (Lgals3 bp), galectin 9 (Lgals9), Ly6a, lymphocyte antigen 6 family member E (Ly6e), lymphocyte antigen 6 family member E (Mlkl), myeloid cell nuclear differentiation antigen (Mnda), 2′-5′ oligoadenylate synthetase 1A (Oas1a), 2′-5′-oligoadenylate synthetase 2 (Oas2), 2′-5′ oligoadenylate synthetase-like 1 (Oasl1), 2′-5′ oligoadenylate synthetase-like 2 (Oasl2), PHF11a, ring finger protein 213 (Rnf213), Rsad2, sterile alpha motif domain containing 9 like (Samd9l), and SP100 nuclear antigen (Sp100) (Figure 4M). Most of these proteins, associated with the regulation of apoptosis, are implicated in B-cell growth and development, the recognition, and initiation of antiviral innate immune responses, and interferon-specific and pro-inflammatory responses.

Validation of DEPs

To determine the credibility of the TMT-based analysis of DEPs, the expression of PHF11 (which was downregulated in both the EFA and EFV groups) was detected by Western blot analysis. This analysis showed that PHF11 levels were downregulated in the EFA group compared to those in the control group, consistent with the data obtained by TMT labeling. Semi-quantitative Western blot analysis of IL-8 expression

Table 2. Intergroup ectopic tissue weight data of mice

Variables	One (mg)	Two (mg)	Three (mg)	Four (mg)	Five (mg)	Six (mg)	Mean (mg, s)
CON	20.6	18.7	63.8	35.8	13		30.38 ± 20.5
EFA	64.8	147.5	102.2	271.8	81.8		133.62 ± 83.21
EFV	192.2	139.7	28.5	65	17.4	15.8	81.60 ± 73.60

demonstrated that IL-8 levels increased in the EFA group (Figure 4N). Collectively, these findings suggest that the proteomic analyses conducted in the present study were sufficient to unveil credible changes in the expression of proteins associated with EMS onset.

DISCUSSION

EMS is a benign gynecological disease with malignant potential. The disease is characterized by infertility or pain such as dysmenorrhea, irregular pelvic pain, intercourse pain, and defecation pain and difficulty and often causes psychological illnesses such as anxiety and depression in patients, severely impairing their quality of life. Unfortunately, the etiology of EMS has not yet been elucidated.

An article published by Deborah et al. in 2020[14] indicated a correlation between different cancer types and specific microbiota, as common bacterial functional features were present in the corresponding tumor environment. In recent years, an increasing number of investigations on microbes and EMS have been conducted; however, no uniform conclusion has yet been reached. Previously, Leonardi et al.[15] systematically evaluated the association between EMS and the microbiome. They searched MEDLINE, Embase, Scopus, and Web of Science databases and obtained 251 studies of interest. After duplicate removal and association determination, full-text reviews of the remaining 33 studies were performed. Finally, 18 studies published between 2002 and 2019 were included, 13 of which were clinical studies that detected various tissue types, including tissues from the intestinal tract, cervix, endometrium, fallopian tube, ovary, and peritoneum, as well as peritoneal fluid, follicular fluid, and menstrual blood. Among these investigations, seven delved into the correlation between EMS and intestinal microbes, and only three studies evaluated the α-diversity and β-diversity of microbes. However, research on the association between microbes and EMS pathogenesis was lacking at the time, and none of the included studies yielded uniform conclusions. Therefore, it is necessary to comprehensively analyze the association between EMS and host microbiota.

This study was the first to use bioinformatics to characterize the microbiota in ectopic/eutopic endometrial tissues and the oral cavity of patients with ovarian endometriotic cysts. At the genus level *Ralstonia* was the most abundant in these tissues, the content of which was nearly twice as high as that in eutopic endometrial tissues. The dominant microbes in oral secretions were cocci, with *Streptococcus* boasting the highest richness. The microbiota composition of ectopic and eutopic endometrial tissues partially overlapped, with similar taxon numbers and diversity, but the richness levels of various taxa were significantly different. Significant differences were observed in both richness and taxon diversity between the oral microbiota and the ectopic/eutopic endometrial microbiota. Comparisons of intestinal microbes revealed that patients with EMS and healthy subjects had similar microbial compositions; however, microbial richness was significantly different between the two groups. In the intestinal microbes of EMS patients, *Enterococcus*, *Pseudomonas*, *Haemophilus*, and *Neisseria* exhibited increased richness, while in healthy controls, the richness of *Bacteroides*, *Escherichia coli*, Firmicutes, *Bifidobacterium*, and *Faecalibacterium* was markedly increased, indicating statistically significant intergroup differences.

The present study compared ectopic and eutopic endometrial tissues rather than the microbiota of peritoneal fluid and external cervical os because the microbiota of the external cervical os is susceptible to the impact of estrogen and environmental and lifestyle factors, as well as the direct influence of the short anal-genital distance, which could induce dysbiosis of the cervicovaginal microflora. However, the female upper genital tract, including the pelvic cavity, fallopian tube, and uterine cavity, protected by a closed cervix and cervical mucus plug, is relatively confined. In this context, as the menstrual blood reflux was the primary inducement of EMS, eutopic endometrial contamination was minimized. Additionally, we analyzed the oral microbes of patients with EMS, performed a more comprehensive analysis of the diversity and relative richness of microbial flora in different body parts of these patients, and reported the richness changes of *Enterococcus* for the first time in the diversity analysis of the intestinal microbes of patients with EMS.

Enterococcus, a Gram-positive coccus, is a common inhabitant of the human gastrointestinal tract. They are core members of the microbiome and can trigger severe infections. *Enterococcus* exhibits intrinsic and acquired antibiotic resistance and limited susceptibility to antibiotics.[16] Currently, vancomycin, linezolid, and tigecycline are effective against *Enterococcus*.[17] Fecal microbiota transplantation has become an effective approach to investigate the relationship between specific diseases and gut microbiota and is a therapeutic option for autoimmune diseases. Nevertheless, fecal microbiota transplantation is insufficient to illustrate the microbiota-disease association because interactions among microbes are intricate, and the modification of fecal transportation on gut microbiota may not lead to complete immune imbalance.[18] Hence, the transportation of explicitly targeted microbes is more convincing. To explore the role of *Enterococcus* in the onset of EMS, *in vitro* animal experiments were performed in the present study. EMS murine models were established by oral gavage of *Enterococcus* colonies (no mice died during the experiments). Using our innovative and feasible experimental method, we discovered that EMS murine models established by gut microbiota gavage exhibited a higher degree of lesion infiltration and more widely distributed lesions, which demonstrates an essential role for *Enterococcus* in the development of EMS.

Subsequently, TMT-based quantitative proteomic analysis was conducted on tissues from these successfully modeled animals. Proteins, as executers of all activities, play a key role in cellular functions. Proteomic analysis based on TMT labeling has the advantage of accurately

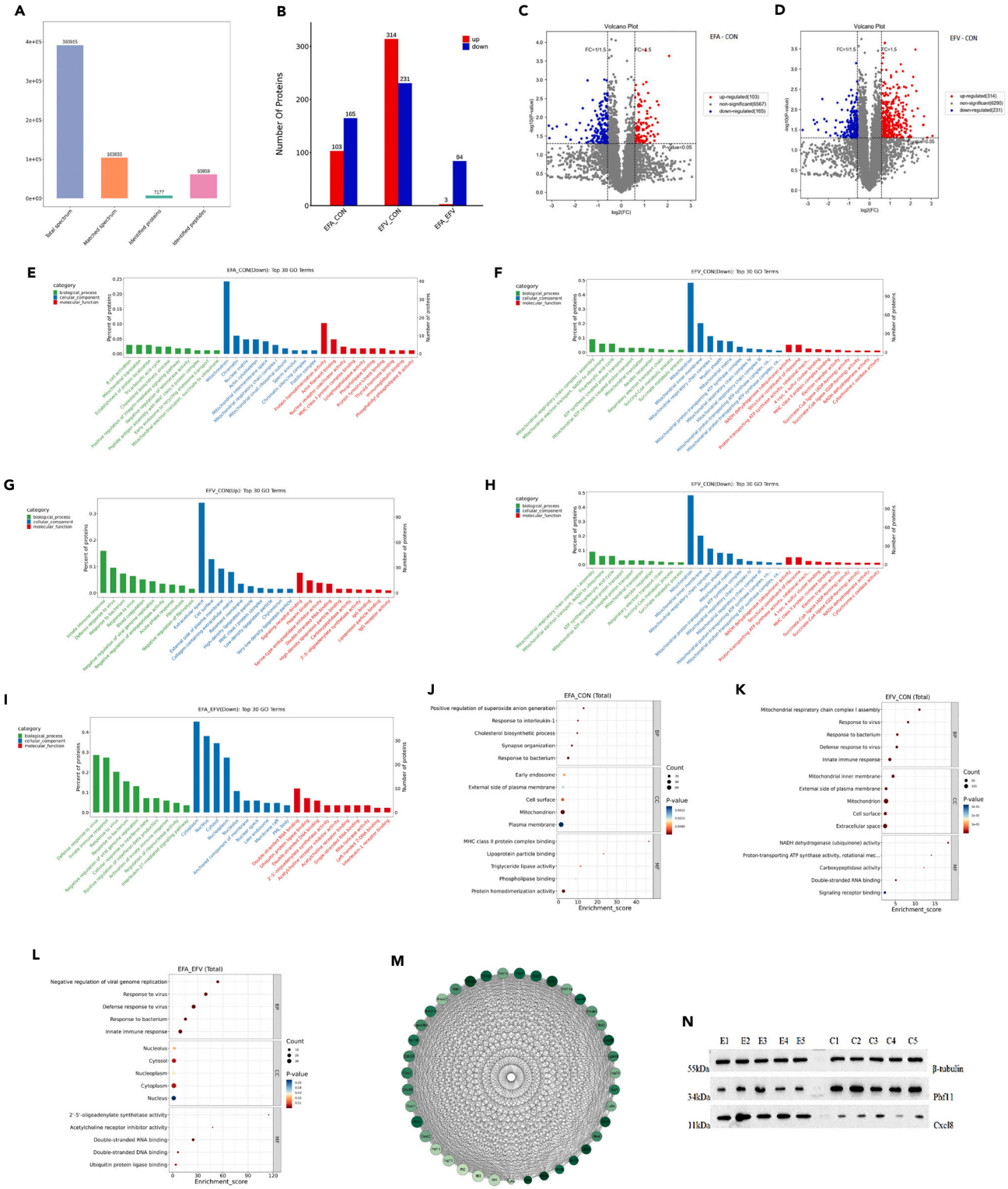

Figure 4. Identification and bioinformatic analysis of DEPs in murine models of Enterococcus-induced lesions

(A) Histogram of basic protein identification results.

(B) Histogram of the different proteins in each group. The horizontal coordinate is the comparison group, the vertical coordinate is the number of different proteins, red represents proteins with upregulated expression, and blue represents proteins with downregulated expression. The horizontal coordinate of the volcano map is log2(FC). The farther its value is from 0, the greater the difference. The right side and left side represent proteins with upregulated and

Figure 4. *Continued*

downregulated expression levels, respectively. The ordinate is -log10(P-value), and the farther the ordinate value is from 0, the greater the difference. The blue dots represent downregulated DEPs, the red dots represent upregulated DEPs, and the gray dots represent non-significantly DEPs (C(EFA-CON), D(EFV-CON); GO enrichment analysis results. The x coordinate represents the name of the GO item, and the y coordinate represents the protein quantity and its percentage of the corresponding item.

(E) Upregulated protein enrichment histogram in the top 30 of EFA-CON.

(F) Downregulated protein enrichment histogram in the top 30 of EFA-CON.

(G) Upregulated protein enrichment histogram in the first 30 EFV-CON.

(H) Downregulated protein enrichment histogram in the first 30 EFV-CON.

(I) Histogram of downregulated protein enrichment in the top 30 of EFA-EFV; KEGG enriched top 20 bubbles, in which the x axis represents the enrichment score and the y axis enrichment score is the pathway information of the top 20. The items with larger bubbles contain more different proteins, and the bubble color changes from blue to red. The smaller the enrichment p value, the greater the significance.

(J) EFA-CON enrichment bubble diagram.

(K) EFV-CON enriched bubble map.

(L) EFA-EFV enriched bubble map.

(M) PPI network diagram representing the interaction relationship network diagram of different proteins.

(N) Western blot analysis was used to verify the DEPs; PHF11 and Cxcl8 expression were decreased in EFA mice.

quantifying relative protein levels in complex samples and has been applied to identify potential disease biomarkers. Among the large number of DEPs identified in our study, the core proteins of the EFA group were primarily downregulated compared with those of the EFV group. Among the top 10 proteins with the most significant downregulation trends, PHF11 was upregulated in the EFV group. PHF11, which is prevalent in 25 human tissues, is mainly expressed in immune cells. Containing a gene related to cytokine activation, PHF11 has multiple functions, including DNA repair. As a polymorphism of PHF11 is correlated with elevated immunoglobulin E (IgE) levels, it has been defined as a candidate gene for asthma in some studies.[19] However, the mechanism of action of PHF11 in this disease has not yet been clarified. Regarding potential PHF11 functions, Clarke et al.[20] noted that the atopy-related genes of PHF11 were regulators of T cells that expressed type 1 cytokine genes through the NF-κB pathway. This pathway is associated with atopy and non-atopy eczema in both murine and human studies. In 2015, Pauline et al.[21] investigated the keratinocyte cell line HaCaT and discovered that the downregulated expression of PHF11 was accompanied by increased expression of IL-8; the decreased expression of PHF11, usually associated with enhanced proliferation and migration, facilitated inflammation and tissue remodeling after infections or tissue injuries. IL-8 is an effective angiogenic agent that can induce the chemotaxis of neutrophils and other immune cells. A considerable body of evidence has demonstrated that IL-8 levels are positively correlated with EMS severity and that IL-8 is implicated in the entire process of EMS development, including the adhesion, invasion, and implantation of ectopic tissues. IL-8 also protects ectopic tissues from apoptosis.[22] To illustrate the association between PHF11 and IL-8 in patients with EMS, we confirmed that the tissues of *Enterococcus*-infected EMS model mice presented visibly decreased PHF11 expression, accompanied by abnormally elevated IL-8 expression.

In the current study, we systematically and comprehensively analyzed the distribution features of the microbiota in different body parts of patients with EMS, identified the differentially distributed microbe *Enterococcus* in the gut microbiota, verified in an animal experiment in which *Enterococcus* infection aggravated the development of EMS, and identified the DEP PHF11 in ectopic tissues. As the downregulated expression of PHF11 was accompanied by the elevated expression of IL-8, we propose for the first time that the presence of *Enterococcus* resulted in the downregulated expression of PHF11 in endometrial tissues and elevate IL-8 levels in ectopic tissues, thereby promoting cell adhesion and growth in the ectopic endometrium, identifying a potential regulatory mechanism for PHF11 in EMS development.

Limitations of the study

This study has some limitations. Owing to functional interference among microbes, biological hypotheses based on microbiome alterations have some limitations. Considering this, future research should be more standardized, include and analyze diverse samples, and adjust the inference factors to compare the results of different studies.

STAR★METHODS

Detailed methods are provided in the online version of this paper and include the following:

- KEY RESOURCES TABLE
- RESOURCE AVAILABILITY
  - Lead contact
  - Materials availability
  - Data and code availability
- EXPERIMENTAL MODEL AND STUDY PARTICIPANT DETAILS
  - Subject enrollment and sample collection
  - Animal model establishment
- METHOD DETAILS
  - 16S ribosomal RNA high-throughput sequencing and data analysis

- Tandem mass tag-labeled quantitative proteomic analysis
- Western blotting
- QUANTIFICATION AND STATISTICAL ANALYSIS

ACKNOWLEDGMENTS

We thank the patient for their participation in this study as well as all the referring physicians.

AUTHOR CONTRIBUTIONS

Y.X.C conceived, designed, and supervised the study. J.J.H, G.J.L designed, performed, and analyzed tissue specimen *in vitro* experiments. G.J.L, M.M.H, H.G performed 16SrDNA amplicon sequencing and analyses. J.J.H, Q.S. S, N.R.X designed, performed and analyzed mouse model experiment. J.J.H, J.Q.Z performed and analyses mouse model. J.J.H, W.J.Y, A.Y.X, X.W designed, performed and analyzed proteomic analysis. J.J.H, Y.W, R.W, C.X analyzed proteomic data. Y.Q.L, Y.F performed Western blotting. X.F.X, H.G supervised experiments and provided critical reagents. J.J.H. wrote the paper, which other authors commented on.

DECLARATION OF INTERESTS

The authors declare no competing interests.

Received: June 21, 2023
Revised: September 25, 2023
Accepted: October 5, 2023
Published: October 7, 2023

REFERENCES

1. As-Sanie, S., Black, R., Giudice, L.C., Gray Valbrun, T., Gupta, J., Jones, B., Laufer, M.R., Milspaw, A.T., Missmer, S.A., Norman, A., et al. (2019). Assessing research gaps and unmet needs in endometriosis. Am. J. Obstet. Gynecol. *221*, 86–94. https://doi.org/10.1016/j.ajog.2019.02.033.
2. Wei, J.J., William, J., and Bulun, S. (2011). Endometriosis and ovarian cancer: a review of clinical, pathologic, and molecular aspects. Int. J. Gynecol. Pathol. *30*, 553–568. https://doi.org/10.1097/PGP.0b013e31821f4b85.
3. Zondervan, K.T., Becker, C.M., Koga, K., Missmer, S.A., Taylor, R.N., and Viganò, P. (2018). Endometriosis. Nat. Rev. Dis. Primers *4*, 9. https://doi.org/10.1038/s41572-018-0008-5.
4. Sampson, J.A. (1927). Metastatic or Embolic Endometriosis, due to the Menstrual Dissemination of Endometrial Tissue into the Venous Circulation. Am. J. Pathol. *3*, 93–110.43.
5. Symons, L.K., Miller, J.E., Kay, V.R., Marks, R.M., Liblik, K., Koti, M., and Tayade, C. (2018). The Immunopathophysiology of Endometriosis. Trends Mol. Med. *24*, 748–762. https://doi.org/10.1016/j.molmed.2018.07.004.
6. McLaren, J., Prentice, A., Charnock-Jones, D.S., Millican, S.A., Müller, K.H., Sharkey, A.M., and Smith, S.K. (1996). Vascular endothelial growth factor is produced by peritoneal fluid macrophages in endometriosis and is regulated by ovarian steroids. J. Clin. Invest. *98*, 482–489. https://doi.org/10.1172/JCI118815.
7. Arici, A. (2002). Local cytokines in endometrial tissue: the role of interleukin-8 in the pathogenesis of endometriosis. Ann. N. Y. Acad. Sci. *955*, 101–109. , discussion 118, 396-406. https://doi.org/10.1111/j.1749-6632.2002.tb02770.x.
8. Smycz-Kubańska, M., Mamrocha, A., Wendlocha, D., Królewska-Daszczyńska, P., Strzelec, A., Stępień, S., and Mielczarek-Palacz, A. (2022). Analysis of the concentration of CXCL8 chemokine and its CXCR1 and CXCR2 receptors in peritoneal fluid of women with endometriosis. Pol. Merkur. Lekarski. *50*, 232–236.
9. Liu, H., Zhang, H., Han, Y., Hu, Y., Geng, Z., and Su, J. (2022). Bacterial extracellular vesicles-based therapeutic strategies for bone and soft tissue tumors therapy. Theranostics *12*, 6576–6594. https://doi.org/10.7150/thno.78034.
10. Davies, J. (2001). In a map for human life, count the microbes, too. Science (New York, N.Y.) *291*, 2316. https://doi.org/10.1126/science.291.5512.2316b.
11. Relman, D.A., and Falkow, S. (2001). The meaning and impact of the human genome sequence for microbiology. Trends Microbiol. *9*, 206–208. https://doi.org/10.1016/s0966-842x(01)02041-8.
12. Liu, R., Zhang, C., Shi, Y., Zhang, F., Li, L., Wang, X., Ling, Y., Fu, H., Dong, W., Shen, J., et al. (2017). Dysbiosis of Gut Microbiota Associated with Clinical Parameters in Polycystic Ovary Syndrome. Front. Microbiol. *8*, 324. https://doi.org/10.3389/fmicb.2017.00324.
13. Witkin, S.S., and Forney, L.J. (2020). The microbiome and women's health: perspectives and controversies. BJOG An Int. J. Obstet. Gynaecol. *127*, 127. https://doi.org/10.1111/1471-0528.16010.
14. Nejman, D., Livyatan, I., Fuks, G., Gavert, N., Zwang, Y., Geller, L.T., Rotter-Maskowitz, A., Weiser, R., Mallel, G., Gigi, E., et al. (2020). The human tumor microbiome is composed of tumor type-specific intracellular bacteria. Science (New York, N.Y.) *368*, 973–980. https://doi.org/10.1126/science.aay9189.
15. Leonardi, M., Hicks, C., El-Assaad, F., El-Omar, E., and Condous, G. (2020). Endometriosis and the microbiome: a systematic review. BJOG An Int. J. Obstet. Gynaecol. *127*, 239–249. https://doi.org/10.1111/1471-0528.15916.
16. Fiore, E., Van Tyne, D., and Gilmore, M.S. (2019). Pathogenicity of Enterococci. Microbiol. Spectr. *7*, 1083–1089. https://doi.org/10.1128/microbiolspec.GPP3-0053-2018.
17. Raza, T., Ullah, S.R., Mehmood, K., and Andleeb, S. (2018). Vancomycin resistant Enterococci: A brief review. J. Pak. Med. Assoc. *68*, 768–772.
18. Bokoliya, S.C., Dorsett, Y., Panier, H., and Zhou, Y. (2021). Procedures for Fecal Microbiota Transplantation in Murine Microbiome Studies. Front. Cell. Infect. Microbiol. *11*, 711055. https://doi.org/10.3389/fcimb.2021.711055.
19. Adcock, I.M., and Kirkham, P.A. (2010). PHF11 and DPP10: a tale of two genes in asthma. Respiration *79*, 14–16. https://doi.org/10.1159/000235972.
20. Clarke, E., Rahman, N., Page, N., Rolph, M.S., Stewart, G.J., and Jones, G.J. (2008). Functional characterization of the atopy-associated gene PHF11. J. Allergy Clin. Immunol. *121*, 1148–1154.e3. https://doi.org/10.1016/j.jaci.2008.02.028.
21. Muscat, P., Mercado, K., Payne, K., Chahal, H., and Jones, G. (2015). PHF11 expression and cellular distribution is regulated by the Toll-Like Receptor 3 Ligand Polyinosinic:Polycytidylic Acid in HaCaT keratinocytes. BMC Immunol. *16*, 69. https://doi.org/10.1186/s12865-015-0131-y.
22. Sikora, J., Smycz-Kubańska, M., Mielczarek-Palacz, A., and Kondera-Anasz, Z. (2017). Abnormal peritoneal regulation of chemokine activation-The role of IL-8 in pathogenesis of endometriosis. Am. J. Reprod. Immunol. *2017*, 77–81. https://doi.org/10.1111/aji.12622.
23. Morgun, A., Dzutsev, A., Dong, X., Greer, R.L., Sexton, D.J., Ravel, J., Schuster, M., Hsiao, W., Matzinger, P., and Shulzhenko, N. (2015). Uncovering effects of antibiotics on the host and microbiota using transkingdom gene

networks. Gut *64*, 1732–1743. https://doi.org/10.1136/gutjnl-2014-308820.

24. Caporaso, J.G., Lauber, C.L., Walters, W.A., Berg-Lyons, D., Lozupone, C.A., Turnbaugh, P.J., Fierer, N., and Knight, R. (2011). Global patterns of 16S rRNA diversity at a depth of millions of sequences per sample. Proc. Natl. Acad. Sci. USA *108*, 4516–4522. https://doi.org/10.1073/pnas.1000080107.
25. Magoč, T., and Salzberg, S.L. (2011). FLASH: fast length adjustment of short reads to improve genome assemblies. Bioinformatics *27*, 2957–2963. https://doi.org/10.1093/bioinformatics/btr507.
26. Edgar, R.C. (2013). UPARSE: highly accurate OTU sequences from microbial amplicon reads. Nat. Methods *10*, 996–998. https://doi.org/10.1038/nmeth.2604.
27. Quast, C., Pruesse, E., Yilmaz, P., Gerken, J., Schweer, T., Yarza, P., Peplies, J., and Glöckner, F.O. (2013). The SILVA ribosomal RNA gene database project: improved data processing and web-based tools. Nucleic Acids Res. *41*, D590–D596. https://doi.org/10.1093/nar/gks1219.
28. Edgar, R.C. (2004). MUSCLE: multiple sequence alignment with high accuracy and high throughput. Nucleic Acids Res. *32*, 1792–1797. https://doi.org/10.1093/nar/gkh340.
29. Kohl, M., Wiese, S., and Warscheid, B. (2011). Cytoscape: software for visualization and analysis of biological networks. Methods Mol. Biol. *696*, 291–303. https://doi.org/10.1007/978-1-60761-987-1_18.
30. Bader, G.D., and Hogue, C.W.V. (2003). An automated method for finding molecular complexes in large protein interaction networks. BMC Bioinf. *4*, 2. https://doi.org/10.1186/1471-2105-4-2.
31. Szklarczyk, D., Gable, A.L., Lyon, D., Junge, A., Wyder, S., Huerta-Cepas, J., Simonovic, M., Doncheva, N.T., Morris, J.H., Bork, P., et al. (2019). STRING v11: protein-protein association networks with increased coverage, supporting functional discovery in genome-wide experimental datasets. Nucleic Acids Res. *47*, D607–D613. https://doi.org/10.1093/nar/gky1131.
32. Yang, P., Tang, W., Li, H., Hua, R., Yuan, Y., Zhang, Y., Zhu, Y., Cui, Y., and Sha, J. (2021). T-complex protein 1 subunit zeta-2 (CCT6B) deficiency induces murine teratospermia. PeerJ *9*, e11545. https://doi.org/10.7717/peerj.11545.
33. Xu, J., Zhang, L., Hou, J., Wang, X., Liu, H., Zheng, D., and Liang, R. (2017). iTRAQ-based quantitative proteomic analysis of the global response to 17β-estradiol in estrogen-degradation strain Pseudomonas putida SJTE-1. Sci. Rep. *7*, 41682. https://doi.org/10.1038/srep41682.

STAR★METHODS

KEY RESOURCES TABLE

REAGENT or RESOURCE	SOURCE	IDENTIFIER
Experimental models: Organisms/strains		
BALB/c mice	Integrated Animals	RRID:APB:4790
72 human tissue and stool specimens	Han population, Asia	N/A
Bacterial and virus strains		
Enterococcus	Microbiologics	Cat#29212
Chemicals, peptides, and recombinant proteins		
High-Fidelity PCR Master Mix	New England Biolabs	Cat#F531L
Ampicillin	Medchemexpress	Cat#HY-B0522
Metronidazole	Medchemexpress	Cat#HY-B0318
Vancomycin	Medchemexpress	Cat#HY-B0671
Ciprofloxacin hydrochloride	Medchemexpress	Cat#HY-B0356
Imipenem	Medchemexpress	Cat#HY-B1369A
Estradiol benzoate	Medchemexpress	Cat#HY-B1192
Dithiothreitol	Merck	Cat#3483-12-3
Iodoacetamide	Merck	Cat#144-48-9
Triethylammonium bicarbonate	Merck	Cat#15715-58-9
Acetonitrile	Merck	Cat#75-05-8
Antibodies		
Anti-Phf11	Proteintech	Cat#10898-1-AP, RRID:AB_2165207
Anti-Cxcl8	Proteintech	Cat#27095-1-AP, RRID:AB_2861340
Anti-β-tubulin	Beyotime	Cat#AF2835, RRID:AB_2250582
Deposited data		
Sequene data	This paper	SUB13792018
Western blotting	This paper	https://doi.org/10.17632/4sh78xh8zh.1
Critical commercial assays		
Bicinchoninic Acid (BCA) Protein Assay	ThermoScientific	Cat#23225
Estain Ig protein staining decolorization concentration kit	GenScript	Cat#L00755C-500
Phosphorylated protein enrichment Kit	ThermoScientific	Cat#A32992
Isobaric Tags for Relative and Absolute Quantitation kit	ThermoScientific	Cat#4381663-1KT
Tandem Mass Tag six kit	ThermoScientific	Cat#90066
Tandem Mass Tag prosixteen kit	ThermoScientific	Cat#A44520
Software and algorithms		
Python3.7.1	Google	https://www.python.org/
Uparse v7.0.1001	Robert Edgar	http://drive5.com/uparse/
MUSCLE version 3.8.31	Robert Edgar	http://www.drive5.com/muscle/
KEGG 102.0	Kanehisa Laboratories	https://www.genome.jp/kegg/pathway.html
STRING 11.5	SIB	https://cn.string-db.org/
R version 4.2.0	The R Foundation	https://www.r-project.org/

RESOURCE AVAILABILITY

Lead contact

Further information and requests for resources and reagents should be directed to and will be fulfilled by the lead contact, Yunxia Cao (caoyunxia5972@ahmu.edu.cn).

Materials availability

This study did not generate new unique reagents.

Data and code availability

All data and methods necessary to reproduce this study are included in the manuscript and supplemental information. Sequencing data were deposited to the National Center for Biotechnology Information under accession number SUB13792018 and Mendeley data under https://doi.org/10.17632/4sh78xh8zh.1 are publicly available. This research does not report original code. Other original data reported in this paper will be shared by the lead contact upon request.

EXPERIMENTAL MODEL AND STUDY PARTICIPANT DETAILS

Subject enrollment and sample collection

This study was approved by the Ethics Committee of the First Affiliated Hospital of Anhui Medical University (No. PJ20160409; No. LLSC20220135), and informed consent was obtained from all participants prior to the trial. A total of 14 patients with endometriotic cysts (the EMS group) and 24 healthy controls (CON group) were included in the study.

The inclusion criteria for the EMS group were as follows: (1) patients aged from 18 to 40 years old; (2) patients with clinical symptoms indicative of EMS (dysmenorrhea, dyspareunia, and insomnia); (3) patients with moderate to severe EMS (stages III-IV, as determined by the revised American Society for Reproductive Medicine [rASRM]) confirmed by laparoscopic biopsy; and (4) patients who had no sexual intercourse within 48 h, did not accept vaginal lavage or medication within 5 days, and underwent no cervical treatment within 1 week. The inclusion criteria for the control group were female patients who underwent laparoscopic surgery for tubal examination and those who had no EMS symptoms observed during surgery or pathological examination. Patients with inflammatory bowel diseases, functional bowel diseases, malignancies, or autoimmune diseases were excluded.

All participants had regular menstrual cycles (28 $\pm$ 2.2 days) and had not accepted hormone therapies, antibiotics, or vaginal drugs for 6 months.

Samples were collected within 3–5 days of menstruation. Four samples from different body parts were obtained from each patient with EMS, including ectopic (EM) and eutopic(EU) endometrial tissues, pharyngeal swabs(OM), and fecal samples(FE). Fecal samples from 24 healthy controls (FE) were also collected. Pharyngeal swabs and fecal samples were collected before treatment. During the collection of pharyngeal swab samples, the posterior pharyngeal wall and tongue were swabbed three times, after which the swab head was quickly inserted into a disposable sampling tube, the end of the swab was discarded, and the tube cap was tightened. For fecal samples, the central part of the stool (3–5 g) was collected in a sterile tube. Ectopic and eutopic endometrial tissues were collected intraoperatively. After disinfecting the cervical canal and vagina with iodine, a vacuum suction tube was inserted into the uterine cavity to collect ectopic endometrial tissues, during which time the tube was not in contact with the vaginal wall or cervix. Subsequently, ectopic tissues pathologically confirmed by biopsy were cut into 1 × 1 cm tissue blocks. Both ectopic and eutopic endometrial tissues were stored in 15 mL Falcon tubes. All samples were transferred immediately after collection and stored at −80°C.

Animal model establishment

Female adolescent BALB/c mice (8-weeks-old) were selected and kept in sterile box cages (5–6 mice per cage) with independent ventilation. Temperature, humidity, pressure difference, illumination, and fan operation were controlled on a computer in real-time, and sterile feed and water were accessible to all mice. All animal testing procedures were approved by the Animal Care and Use Committee of Anhui Medical University in accordance with China's animal care regulations. Following one week of adaptive feeding, the mice were randomized into donor and recipient mice groups, and the recipient mice were further stratified randomly into three groups: control (CON; no intervention), aseptic treatment with gavage of *Enterococcus* suspension (1 × 10^9 CFU) (EFA), and aseptic treatment with gavage of *Enterococcus* suspension (1 × 10^9 CFU) and vancomycin treatment (500 mg/L) (EFV). During aseptic treatment, recipient mice were orally administered a mixture of Ampicillin and Metronidazole (1 g/L), vancomycin (500 mg/L), ciprofloxacin hydrochloride (200 mg/L), and imipenem (250 mg/L)[23] by gavage for 14 consecutive days. Following blood plate inoculation, *Enterococcus* strains were cultured in a biochemical incubator (37°C, 24 h) and then passaged. At this point, the *Enterococcus* strains were collected and well mixed with normal saline (NS) to prepare a suspension of 2 × 10^{10} CFU/mL (measured by the bacterial turbidity meter), 0.05 mL of which was finally taken for gavage. Donor mice were subcutaneously injected with estradiol benzoate (3 μg/each) and euthanized by cervical dislocation one week later. Their uteri were separated in phosphate-buffered saline (PBS) and scissored into uniform fragments less than 1 mm in length. The endometrial fragments of two donor mice were mixed and injected evenly into three recipient mice using a 1-mL syringe and a 20-mL needle. Three groups of recipient mice were subjected to different gavage treatments. After seven continuous days of gavage, the mice were dissected and endometriotic lesion tissue samples were collected, which were frozen and stored at −80°C. No mice died during the experiment.

METHOD DETAILS

16S ribosomal RNA high-throughput sequencing and data analysis

Total genomic DNA was isolated from the samples using cetyltrimethylammonium bromide, and DNA concentration and purity were measured on a 1% agarose gel. DNA at different concentrations was diluted to 1 ng/μL with sterile water, followed by amplification of different regions (V3-V4) of the 16S ribosomal RNA (rRNA) genes using specific primers with a barcode. All polymerase chain reactions (PCRs) were carried out using 15 μL PhusionHigh-Fidelity PCR Master Mix (New England Biolabs), 2 μM each of the forward and reverse primers, and 10 ng of template DNA. Thermal cycling was performed in the following steps: initial denaturation (98°C, 1 min), denaturation (98°C, 10 s), annealing (50°C, 30 s), and extension (72°C, 30 s).[24] Finally, incubation at 72°C was conducted for 5 min 1X loading buffer (containing SYBR green) and the PCR products were mixed and electrophoresed on a 2% agarose gel. The PCR products were mixed at equal density ratios, after which the mixture was purified using a Qiagen Gel Extraction Kit (Qiagen, Germany). Sequencing libraries were established using the TruSeq DNA PCR-Free Sample Preparation Kit (Illumina, USA) according to the manufacturer's recommendations, and index codes were added. The quality of the libraries was estimated using a Qubit 2.0 Fluorometer (Thermo Scientific) and an Agilent 2100 Bioanalyzer system. Finally, the libraries were sequenced on the Illumina NovaSeq platform, which yielded 250 bp paired-end reads. Sequence analysis was performed using Uparse software (Uparse v7.0.1001, http://drive5.com/uparse/),[25] with sequences of ≥97% similarity categorized into the same operational taxonomic unit (OTU). Subsequently, the representative sequences of each OTU were screened out for further annotation.[26] To investigate the phylogenetic relationships among different OTUs and the differences in the dominant species in different samples (groups), multiple sequence comparisons were performed using MUSCLE software (version 3.8.31, http://www.drive5.com/muscle/).[27] An α-diversity analysis was performed to analyze the complexity of species diversity in our samples using six indicators (observe-species, Chao1, Shannon, Simpson, abundance-based coverage estimators (ACE), and good coverage). All indicators were calculated using QIIME (version 1.7.0) and displayed using R software (version 2.15.3). In addition, a β-diversity analysis was conducted to evaluate differences in sample species complexity, and β-diversity in weighted and unweighted UniFrac was calculated using QIIME. Prior to cluster analysis, principal component analysis (PCA), followed by principal coordinate analysis (PCoA), was performed to obtain and visualize the principal coordinates from complicated multidimensional data. Both PCA and PCoA were displayed using the ade4 and ggplot2 packages using R software (version 2.15.3). Parameter and non-parameter tests were performed. The t-test and Wilcox test were conducted for two groups, whereas for more than two groups, Tukey's test and Wilcox test of the Agricola package were carried out. Differences were considered significant when the P-values were ≤ 0.05.[28]

Tandem mass tag-labeled quantitative proteomic analysis

Protein extraction and digestion

Frozen samples (approximately 100 mg each) were ground in liquid nitrogen into a homogeneous powder, which was homogenized in 1 mL of phenol extraction buffer. Subsequently, 1 mL of saturated phenol and Tris-HCl (pH 7.5) were added. The mixture was held for 30 min at 4°C and centrifuged for 10 min (4°C, 7100 ×*g*). The supernatant was collected and mixed with ammonium acetate and methanol. After overnight storage at −20°C, a second centrifugation (4°C, 12000 ×*g*, 10 min) was conducted to precipitate protein pellets, which were resuspended twice with pre-chilled methanol and ice-cold acetone. After a third centrifugation, the pellets were collected, air-dried, and resuspended with 300 μL lysate. Following a 3-h incubation period at room temperature, the supernatant was collected and the bicinchoninic acid method was used to determine the total protein concentration. Based on the measured concentration, an appropriate amount of protein was diluted to the same concentration and volume. A corresponding volume of 25 mM dithiothreitol was added to the concentration of about 5 mM, followed by an incubation of 30–60 min at 55°C. Iodoacetamide was added to the final concentration of about 10 mM, and the mixture was placed in the dark at room temperature for 15–30 min, which was later added with a 6-fold volume of pre-cooled acetone and placed at −20°C for 4 h to precipitate the proteins. After centrifugation (4°C, 8000 ×*g*, 10 min), the precipitate was collected and re-dissolved in an enzymolysis dilution (protein:enzyme = 50:1 [m/m], 100 μg proteins +2 μg enzymes), which was followed by a 12-h incubation period at 37°C for enzymolysis.

Tandem mass tag/isobaric tags for relative and absolute quantification labeling and liquid chromatography-mass spectrometry

For tandem mass tag (TMT)/isobaric tags for relative and absolute quantification (iTRAQ) labeling, 30 μL of 100 mM triethylammonium bicarbonate (TEAB) were used for labeling, which was mixed with acetonitrile and the TMT/iTRAQ labeling reagents at room temperature. After 1-h of incubation at room temperature, 5% hydroxylamine was added, followed by a 15-min incubation period to stop the reaction. The labeled peptide solution was freeze-dried and stored at −80°C. Reversed phase (RP) separation was conducted on a 1100 HPLC system (Agilent) using an Agilent Zorbax Extend RP column (5 μm, 150 mm × 2.1 mm). Mobile phases A (2% acetonitrile in high-performance liquid chromatography [LC] water) and B (98% acetonitrile in high-performance LC water) were applied to the RP gradient. The solvent gradient was set as follows: 0–8 min, 98% A; 8–8.01 min, 98–95% A; 8.01–48 min, 95–75% A; 48–60 min, 75–60% A; 60–60.01 min, 60–10% A; 60.01–70 min, 10% A; and 70–70.01 min, 10–98% A; a flow rate of 300 μL/min was used, and detection was carried out at 210 nm. The sample collection duration was 8–60 min. The separated peptides were lyophilized for mass spectrometry using a Q Exactive HF mass spectrometer (Thermo Fisher Scientific) equipped with a Nanospray Flex source (Thermo Fisher Scientific).[29,30]

Database search

All raw data from the UniProt *Mus musculus* database were retrieved using ProteomeDiscoverer (v.2.4). The retrieval conditions were as follows: keyword, trypsin digestion specificity; fixed modification, cysteine alkylation; protein quantification approach, TMT/iTRAQ; global false discovery rate (FDR), 0.01; and protein groups considered for quantification, at least 1 peptide.[31]

Western blotting

Tissue proteins from donor and recipient mice were separated using 12% sodium dodecyl sulfate-polyacrylamide gel electrophoresis (SDS-PAGE), transferred to a polyvinylidene fluoride membrane using a Bio-Rad semi-dry blotter, and kept on the membrane for 60 min. The membrane was blocked with 2.5% skim milk powder and slowly shaken on a shaker and closed for 2 h at room temperature, followed by an overnight incubation period at 4°C with the following primary antibodies: anti-Phf11 (Proteintech, 10898-1-AP, 1:1000), anti-Cxcl8 (Proteintech, 27095-1-AP, 1:1000) and anti-β-tubulin (Beyotime, Af2835-200 μL, 1:2000). Subsequently, the membrane was washed with TBS-Tween-20 (0.1%) three times (10 min each time), incubated with secondary antibodies at 4°C for 2 h,[32] and once again washed with TBS-Tween-20 (0.1%) three times (10 min each time). Finally, enhanced chemiluminescence (ECL) detection reagent (Thermo Scientific) was used, and the protein blotting detection SuperSignalWest Femto Chemiluminescent Substrate (Thermo Fisher Scientific) system was employed to detect protein bands.

QUANTIFICATION AND STATISTICAL ANALYSIS

Using a t-test, differentially expressed proteins (DEPs) were assessed with a fold change (FC) of ≥ 1.5 or $\leq 1/1.5$ and p value of <0.05, and all the identified proteins were labeled via Gene Ontology (GO) (http://www.blast2go.com/b2ghome; http://geneontology.org/) and Kyoto Encyclopedia of Genes and Genomes (KEGG) (http://www.genome.jp/kegg/) pathways. Furthermore, GO and KEGG enrichment analyses were carried out on DEPs, and protein-protein interaction (PPI) analysis was performed via the String database (https://string-db.org/).[33]